Contents lists available at ScienceDirect

Engineering Failure Analysis

journal homepage: www.elsevier.com/locate/engfailanal

Influences of tram characteristics on wheel polygonal wear evolution

Florian Zehetbauer *, Johannes Edelmann, Manfred Plöchl

Institute of Mechanics and Mechatronics, TU Wien, 1060 Vienna, Austria

ARTICLE INFO

ABSTRACT

Out-of-round railway wheels continuously excite the vehicle-track system resulting in fluctuating contact forces, creepages and contact patch dimensions. Accompanied wear may influence the evolution of railway wheel polygonization significantly. Especially in curves with a small radius of curvature, which are typical for tramway networks, considerable wear originates due to high lateral creepages. Long-time wear development studies with dominant polygonal orders reveal that some wavelengths of the wheel enlarge rapidly, whereas others are nearly unaffected or even suppressed. Therefore, fundamental research on significant influences on wheel polygonal wear evolution is required. A representative generic system model of a two-axle tram bogie is set up, and a suitable wear model is implemented to study the polygonal wear evolution at trams. It has been found that structural modes can dominate wheel polygonal wear evolution. In particular, the compliance and interaction of the wheelset axle and the resilient wheel may be essential. Evolution tendency curves are presented, and influences on the wheel polygonization are discussed. Wheel–rail contact conditions and related creepage–creep force characteristics appear to be decisive for the evolution directions and evolution speeds.

1. Introduction

Polygonal wheels with periodic irregularities along the wheel circumference superimposed to a constant wheel radius are a fundamental problem in rolling stock. They are widely found in a broad range of rolling stock vehicles, including metro trains, high-speed vehicles, locomotives, freight wagons and trams. The phenomenon affects the dynamic characteristics of railway wheelsets, especially in the vertical direction, and may have a detrimental influence on ride comfort, vehicle/track components, and life cycles of the wheels.

Multiple generation mechanisms have been investigated as a potential cause of wheel polygonization. Nielsen et al. summarize in [1] the state-of-the-art until 2003. The survey reports on why out-of-round wheels develop and categorises different types of defects on railway wheel treads. In the review paper [2], periodic defects of the wheels, simulation methods of wheel polygonization evolution and remedies to reduce wheel polygonization are addressed. Focus is given to wheel polygonization in metro vehicles, locomotives, and high-speed trains in China. Wheel polygonization and rail corrugation occurring at Chinese high-speed railway systems is discussed in terms of their characteristics, consequences, countermeasures, and formation mechanisms in [3]. A recent paper by Iwnicki et al. [4], presents the main theories for the formation mechanisms, reviews the current measurement methods and computer simulation techniques and discusses the effects and potential mitigation methods.

A majority of scientific researchers consider wheel polygonization to be induced by a 'fixed-frequency' or a 'fixed wavelength' mechanism related to a resonance of the vehicle–track dynamic system. Factors such as material hardness [5], initial imbalances

of the wheelset [6,7], wheel flats [8], wheelset flexibility [2,9,10], local rail flexibility [11–13], self-excitation [14–16], and P2 resonance [2,17–19] have been acknowledged to influence the development of wheel polygonization. The literature suggests that there might not be a universal explanation for the formation and growth of polygonal wheels; it may depend on the (different) types of rolling stocks.

Tram systems display, in comparison to other railway transport industries, unique characteristics that may influence the evolution of polygonal wheels significantly. Due to the complex operating environment of tramway networks, a typical operation route contains a great variety of curves with a small radius of curvature, where intensive wear development is expected. Whereas conventional railway vehicles use almost exclusively solid-axle wheelsets, independently rotating wheels (IRW) are frequently applied in trams. The use of wheelsets in the axlebridge design with IRW, as shown in Fig. 2 later, may allow consistently flat floors in the car body of low-floor trams. Moreover, IRW might impact the evolution of predominant polygonal orders, as the release of the rotational constraint between the two wheels reduces the longitudinal creepage essentially when a vehicle negotiates through curves. Resilient wheels, frequently used on trams to reduce railway rolling noise, might be another interesting feature as their flexibility may impact the wheel–rail interaction significantly [20]. Similar to [16], the combination and interaction between the resilient wheel and the elastic wheelset might amplify the evolution of polygonal wheels.

Long-time wear development studies with dominant polygonal orders reveal that some wavelengths of the wheel enlarge rapidly, whereas others are nearly unaffected or even suppressed [2]. Wheel polygonization might develop from an initial, small amplitude wheel out-of-roundness (OOR), present on the running surface of railway wheels, even when they are new, to more significant radius deviations with dominant orders due to wear in the wheel–rail interface [21]. In situations where other excitation mechanisms (e.g. track excitation, self-excitation) emerge, the contribution of initial wheel OOR may not play a dominant role. However, the impact of the specific phenomenon on the wear evolution will depend on their duration and how often they occur. Moreover, if the excitation mechanism does cause a wavelength, which cannot be exactly divided into the wheel circumference, a polygonal wheel may not form easily [22]. Even if the excitation divides precisely into the wheel circumference, the nominal wheel radius will decrease continuously. An exact division will not last for a long time at a constant speed. In contrast, wear development caused by initial wheel OOR is strictly periodic for every wheel revolution and will be focused on here.

Initial wheel OOR can be assumed as a spectrum with wavelengths in a relevant interval. It acts as a continuous excitation in the vehicle-track system resulting in fluctuating contact responses. At certain frequencies, these responses and thus also wear, will be higher than at others. A key indicator determining whether a certain wavelength will be enlarged or diminished is the phase shift between the wear and the initial radius deviation. Depending on this phase shift and the speed of the train, certain OOR orders might develop dominantly. However, only little attention in scientific literature has been given to the influences of tram characteristics on wheel polygonal wear evolution so far. To address this, railway wheel wear development as a consequence of small initial wheel radius deviations will be the focus of this paper to understand the fundamental phenomena of polygonal wheel evolution at trams.

Enlargement phenomena at out-of-round wheels may be investigated by means of field measurements or numerical simulations. A frequently applied method, e.g. [18,23], used for the prediction of the wear evolution is a concept of a feedback loop – a simulation scheme of short-time dynamics coupled to a long-term wear model. In this procedure, the wheel radius deviations are modified by the wear and included in the new input data before each iteration. Peng et al. [22] introduced a method for wear prediction by means of evolution tendencies curves (ETCs) without conducting a closed-loop simulation scheme. Influences on the evolution of predominant OOR orders at trams will be discussed by their means.

The next section will present the structure of the implemented simulation scheme and a brief introduction of the applied wear prediction method. Additionally, a representative generic system model of a two-axle tram bogie will be introduced. In Section 3.1, structural modes that dominate the ETCs and a formation of potentially predominant polygonal orders will be revealed, and their significance on the acceleration of wear evolution will be highlighted. Emphasis will be put on curved tracks with small radius of curvature. The impact of contact conditions on the ETCs will be studied in Section 3.2. The influence of IRW will be pointed out before final concluding remarks will be drawn.

2. Method for wear prediction

A prediction method without conducting the iterative loop program structure is presented by Peng et al. in [22]. This concept is useful for predicting OOR orders that would grow predominantly at a given speed and is adopted here to study evolution tendencies in curves with a small radius of curvature at trams. A schematic representation of this method is shown at the top of Fig. 1. It consists of four main steps, described in the following:

Input: An initial wheel OOR is provided for the MBS simulation by defining the wheel radius deviation over the wheel rolling angle. In this study, the wheel profile varies only in the radial direction, and the wear is assumed to be equally distributed across the transverse direction. In other words, the transverse profile is assumed not to change.

MBS simulation: A simulation of a dynamic vehicle-track interaction with pre-defined operational conditions (wheel/ rail profile, track design, train speed, axle load, contact conditions) is performed where the time history of contact forces, creepages, and contact geometries is computed. The wheel tread and rail geometries remain constant, as it is assumed that the wear of the profiles is negligible during this short-time computation.

A generic system model of a two-axle tram bogie, see Fig. 2, is used to study the vehicle/track interaction. This model was presented in [24] and is described here briefly. Only a single, non-driven, low-floor tram vehicle is considered as the typical series of driven and non-driven modules is separated. The bogie includes two wheelsets in axlebridge design with independently rotating,
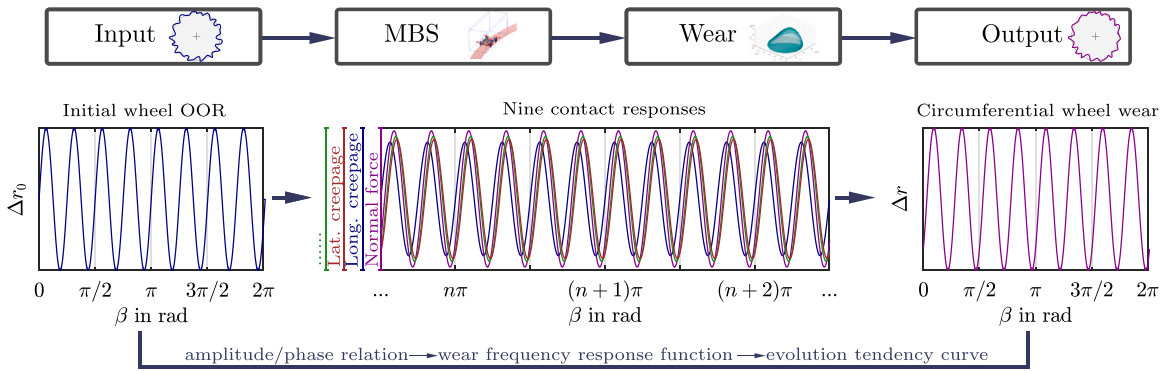
Fig. 1. Method for wear prediction. Top: Simulation scheme. Bottom: Amplitude and phase relation between initial wheel OOR, contact responses, and wear.
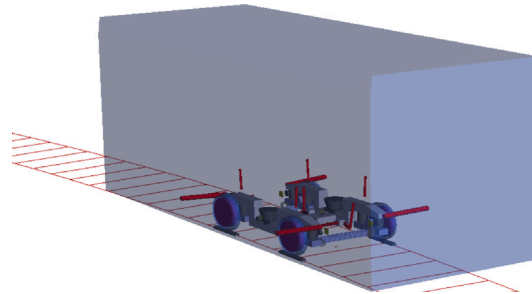

Fig. 2. System model of the tram bogie and car modelled applying the multibody simulation software package SIMPACK.
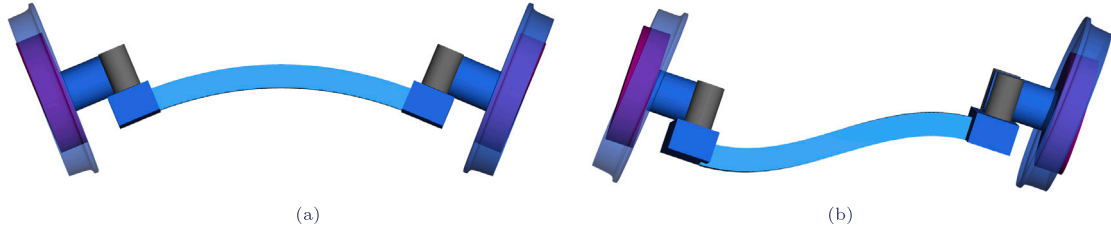

Fig. 3. Flexible mode shapes of the wheelset (a) 1st bending mode (b) 2nd bending mode.

resilient wheels. The model is set up applying the multibody simulation software package SIMPACK [25]. The bogie frame is located below the centre of the car body. Both are modelled by rigid bodies and connected by bushing elements that represent the secondary springs and dampers. Omitted fore and aft cars are substituted by the additional support of the car body against the inertial system w.r.t. pitch and roll by torsional spring–damper elements.

The flexibility of the wheelsets in axlebridge design is accounted for by a linear SIMBEAM element [25]. The wheel hub and the wheel rim of the IRW are represented by rigid bodies; the elastic layer is modelled using a spring–damper element allowing for relative translational and rotational motion of the rim w.r.t. hub in several directions. The modal shapes of the 1st bending mode (21 Hz) and the 2nd bending mode (50 Hz) are illustrated in Fig. 3. Note, it is not the intention to faithfully replicate the modal response of a specific wheelset than rather on generic but representative characteristics to work with. The primary suspension isolates the wheelsets from the bogie frame and is also modelled utilising bushing elements. The main parameters of the generic model are listed in Table 1. Hertzian contact theory [26] is used to derive normal forces. A modified FASTSIM algorithm [27] utilizing the Polach method [28] to consider the contact velocity dependent friction potential is used, [25], to calculate creep forces in wheel–rail contact problem. The track flexibility has not been considered.

Wear model: Wear models in railway applications have been studied for a long time, and several wear models exist. In [29], existing popular wear models are compared. As conclusion, good agreement between the different models was found.

In this study, the KTH (Royal Institute of Technology) wear model [30,31] is utilized to compute the wear. It is a local wear model combining the Archard's wear model [32] and the simplified contact theory by Kalker [27]. Nine contact responses, creepages (longitudinal, lateral, and spin), normal force F_N, Kalker coefficients (C_{11}, C_{22}, and C_{23}), and the contact patch size (semi-axis a and

Table 1
Main system model parameters.

Parameter	Value	Unit
Wheelset mass	850	kg
Car body mass	13000	kg
Wheel radius	0.3	m
Longitudinal stiffness of primary suspension	5.3e6	N/m
Lateral stiffness of primary suspension	5.3e6	N/m
Vertical stiffness of primary suspension	2.2e6	N/m
Longitudinal damping of primary suspension	1.6e4	Ns/m
Lateral damping of primary suspension	1.6e4	Ns/m
Vertical damping of primary suspension	1e4	Ns/m
Effective stiffness coefficient of wheelset axle	5.2e7	N/m
Radial stiffness of resilient wheel	280e6	N/m
Axial stiffness of resilient wheel	160e6	N/m
Deflection stiffness of resilient wheel	3.5e6	Nm/rad
Torsional stiffness of resilient wheel	1.5e6	Nm/rad
Loss factor	0.15	–

b), are required as input, where only abrasive wear mechanisms are accounted for. Main parameters of the wear model are taken from [18].

A wear representation value at the contact patch is obtained based on the approach presented in [29]. As a first step, the wear is accumulated longitudinally. Then, the sums are averaged over the lateral direction. To obtain the longitudinal position of a single wear value at a contact patch, the distances to the maximum wear are averaged longitudinally. The lateral positions are not taken into account, as it is assumed that the wear is equally distributed across the transverse direction.

Output: The wear is interpolated to be discretised in a number of points where wear will be estimated and cumulated around wheel circumference profile. To increase the accuracy of the wear prediction, the wear is accumulated and averaged by a defined number of wheel revolutions.

The method assumes a linear system behaviour between the initial wheel OOR and the circumferential wheel wear, even though the system dynamics contain non-linear elements. This assumption is limited to small wheel radius deviations. In particular, assuming an initial wheel radius deviation, Δr_0, with a single harmonic order over the wheel rolling angle, β, and a track without any irregularities, all contact responses will fluctuate with the excitation frequency of the initial harmonic order, though in different phases, see bottom of Fig. 1. A final phase shift with respect to the initial harmonic wheel deviation emerges for the circumferential wheel wear, Δr, as it still fluctuates with the same (initial) frequency. The wear model introduces the phase relationship between the contact responses and the wear — the steady-state value, the phase shift, and the amplitude of its input, i.e. the individual contact responses, will influence this relationship. Although the growth ratio of the wheel OOR is determined by the amplitude ratio and the phase between the initial wheel radius deviation and the circumferential wheel wear, in reality, the amplitude ratio is extremely small for one wheel revolution. As a consequence, the phase will be the main factor determining the evolution tendency of the wheel OOR (to grow or diminish). If the phase between circumferential wheel wear and the initial wheel OOR is within 90° to 270° range, the initial OOR will grow. Otherwise, it will diminish. At 180°, it reaches its maximum. Note, mean values of the initial OOR orders and circumferential wheel wear are not considered, as only their fluctuation will determine the evolution of the wheel OOR.

Linear superposition of excitation frequencies is possible due to the assumption of linear system behaviour. With this in mind, the amplitude and phase relation between the excitation, i.e. initial wheel OOR, and the circumferential wheel wear can be interpreted as the wear frequency response function in the frequency range of interest. The ETC is obtained from the wear frequency response function and provides information about the polygonal wear evolution. Wheel OOR grows at positive values of the ETC and diminishes at respective negative values at each excitation frequency in the considered range. As pointed out above, the phase between the circumferential wheel wear and initial wheel OOR is the key parameter to determine its evolution direction. The evolution tendencies are normalised as only the comparison of different frequencies and scenarios is significant. A higher absolute value of the evolution tendency means a faster evolution speed. As a consequence, it is expected that distinctive peaks in the ETC will lead to orders that will grow predominant at a given vehicle speed. More details on the wear prediction method can be found in [22].

Growing and diminishing wheel orders can be identified in good approximation at a given vehicle speed with the relationships

$$\lambda = \frac{2\pi R}{\theta} \qquad v = \lambda f \tag{1}$$

where λ is the wavelength, R is the wheel radius, θ is the polygonal order, v is the forward velocity of the wheel, and f is the excitation frequency.

Previous research with ETCs was primarily focused on straight tracks [22,33]. Different and/or phase-shifted radius deviations between the wheels of a bogie were not emphasized but might influence the wear evolution significantly [34]. Especially, an interaction between the left and the right wheel of a single wheelset may be evident. Although significantly weaker, an interaction between the front and the rear wheels of a bogie may also be noticed as vibrations propagate along the flexible track or the flexible bogie.
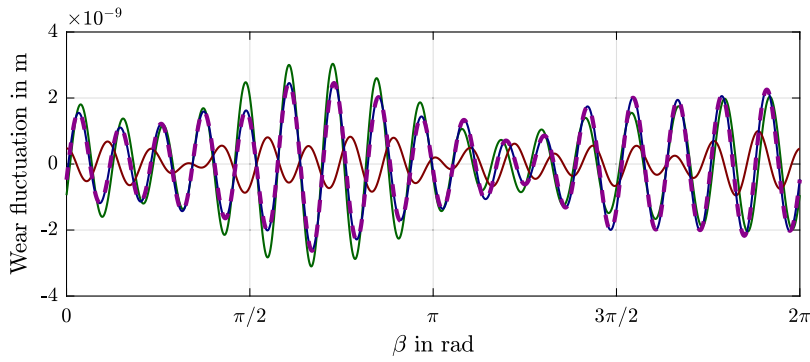
Fig. 4. Linearity analysis of the fluctuation of the wear at the inner wheel caused by random wheel OOR at the inner and outer wheel of the leading wheelset caused by initial OOR inner wheel (———), caused by initial OOR outer (———), caused by both wheels simultaneously (———), linear sum of individual wheels (———).

At IRW, the angular phase shift between the individual wheels changes permanently, and excitations from other wheels can be viewed as random. They may not influence the ETCs. As a consequence, evolution tendencies are considered individually for the respective wheel. However, at solid axle wheelsets or when the angular velocities of the front and rear wheels of each side of the bogie are coupled by means of a gearbox, the phase between the wheels does not change — an impact on the ETCs may be expected and has to be addressed.

An ETC presents the OOR evolution of an individual wheel with respect to an excitation phenomena. To study the influence of several excitation phenomena, a superposition of ETCs is necessary, which requires the assumption of a linear system behaviour between the wheel wear and the respective excitation phenomena. Simulations in curves with a small radius of curvature revealed that the wear caused by random wheel OOR at different wheels of a bogie simultaneously is a simple (linear) sum of those caused by them individually, despite the presence of non-linear elements in the system dynamics.

Fig. 4 presents the fluctuation of the wear at the inner front wheel caused by the outer and the inner wheel of the front wheelset while a vehicle negotiates a curve with a small radius of curvature. Different arbitrary sets of polygonal wheel orders (1–25) and small amplitudes ($\leq 10^{-5}$ m) are featured at both wheels. Only fluctuating components of the wheel wear are addressed, as the mean values of the wear will not influence the OOR evolution. The solid green line is the fluctuation of the wear at the inner wheel caused by the initial wheel OOR at the inner wheel alone and the solid brown curve depicts that caused by the initial wheel OOR at the outer wheel alone. The dashed purple curve is their (linear) sum. The solid blue line represents the fluctuation of the wear at the inner wheel caused by the initial wheel OOR at the inner and outer wheels simultaneously. From Fig. 4 it becomes obvious that the linear addition of the wear fluctuation, dashed purple line, matches the simulation considering both wheels simultaneously, solid blue line, very well.

Consequently, an assumption of the linear system behaviour between the wheel wear and the initial wheel OOR between different wheels of a bogie is feasible, and an analysis of the influence of the different wheels of a bogie on the wear evolution by means of evolution tendencies is possible. An ETC of a wheel is built by superimposing the ETC caused by the analysed wheel itself and the ETC caused by a wheel, which has a constant phase relationship (e.g. solid axle wheelset or coupled by means of a gearbox) with the analysed wheel. Note, in order to do so, it is necessary to identify the angular phase shift between the wheels for each individual wheel OOR frequency or consider appropriate assumptions.

3. Results and discussion

3.1. Influence of structural modes on the wear evolution

To study the influence of the structural modes on the wear evolution, above presented method has been applied considering straight tracks and curved tracks of R $\in \{25, 60, 120, 200, 600\}$ m, where the vehicle model runs on an ideal track and is excited by the initial wheel OOR only. Moreover, seven vehicle configurations, four variants of creep force–creepage characteristics and two different wheel profiles have been investigated. This paper focuses on curves with small radii of curvature, typical for tram networks. For brevity, only the results from R=60 m are presented and discussed. These results are representative w.r.t. curves with a small radius of curvature.

Fig. 5 shows the ETCs at the outer and inner front wheel for four model configurations of the wheelset flexibility. The configurations are listed in Table 2 and allow to allocate the influence of the compliance of the wheelset axle and the resilient wheel, respectively, w.r.t. the OOR evolution. ETCs can either be obtained by sweeping the wheel velocity with a fixed harmonic wavelength excitation or by changing the fixed harmonic wavelength of the excitation at a fixed velocity for a multitude of simulations. Here, the latter was applied. The ETCs are plotted by changing the initial wheel OOR orders to cover the frequency in the considered range with a vehicle speed set to obtain normal accelerations close to 0.65 m/s² For curves with a radius of curvature of R = 60 m the vehicle speeds is close to 22.5 km/h. The fixed harmonic wavelengths with an amplitude of 10^{-6} m are exactly divided by the
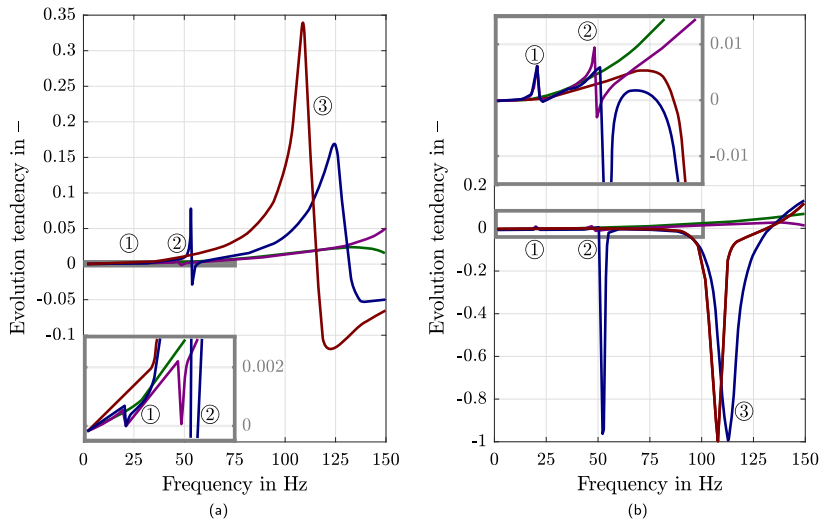
Fig. 5. Influence of the wheelset flexibility on the ETC. (a) Outer front wheel (b) Inner front wheel including detail (grey box). Configuration A (——), Configuration B (——), Configuration C (——), Configuration D (——).

Table 2
Model configurations of the wheelset flexibility.

Configurations	Wheelset axle model	Resilient wheel model
A	Rigid	Rigid
B	Rigid	Flexible
C	Flexible	Rigid
D	Flexible	Flexible

wheel circumference (order 1–45). A normal acceleration of 0.65 m/s^2 is assumed as a typical normal acceleration for trams in curves with small radius of curvature.

Note, the ETCs are normalized with the intent that the highest absolute value of the evolution tendencies is located at one. Based on Eq. (1), the orders corresponding to the frequencies at a given speed can be calculated. As pointed out above, if the evolution tendencies are above zero, the initial respective OOR orders tend to grow. Otherwise, the orders will diminish. A higher absolute value of the evolution tendency is interpreted as a faster evolution speed, and distinctive positive peaks may lead to predominant polygonal orders at a given vehicle speed.

The gradual increase of evolution tendencies with growing frequencies is identified at the rigid wheelset, Configuration A, green line, at the inner wheel. At the outer wheel, evolution tendencies also increase gradually until 134 Hz. From this point, they decrease slightly for the remaining frequencies in the range of interest. As a result, uniform wear without the formation of a predominant polygonal order in the considered frequency range may be expected.

In contrast, at Configuration D, blue line, where both the wheelset axle and the resilient wheel are considered flexible, the evolution tendencies fluctuate between two peaks at about 20 Hz ①, 55 Hz ②, and 120 Hz ③. ① – ③ correspond to distinctive peaks in the wear amplitude response. However, depending on the wear phase response, positive or negative evolution tendencies and related dominant frequencies appear in the ETCs. Particularly, at the outer wheel, Fig. 5(a), the evolution tendencies are negative for low frequencies until the turning point at 6 Hz. From there, they grow gradually until the first positive peak at 19.6 Hz. Now, the tendencies decrease drastically to values close to zero before they start to increase again. At 53.3 Hz the second peak can be identified. Next, the evolution tendencies turn direction at 53.5 Hz and the first negative peak is observed at 53.9 Hz. This is followed by the point at 56.6 Hz where the tendencies turns their direction and the evolution tendencies grow until the third positive peak is reached at 123.5 Hz. Finally, evolution tendencies turn negative at 131 Hz, and corresponding initial OOR orders will dimmish for the remaining frequencies in the range of interest. At the inner wheel, Fig. 5(b), a gradual increase of the evolution tendencies are identified at low frequencies until the first positive peak is at 20 Hz. Then, they decrease drastically towards negative values before the increase again to the second peak at 50.5 Hz. Next, the evolution tendencies turn direction at 51.4 Hz and the first negative peak is observed at 53.4 Hz. It is followed by an area of positive tendencies in the range from 59.4 Hz to 78.3 Hz and another positive peak at 69.5 Hz. The second negative peak is at 112.5 Hz. Finally, the evolution tendencies turn positive at 134.8 Hz and from this point, corresponding initial OOR orders will grow in the frequency range of interest. ① and ② can be associated with the first and second bending modes of the wheelset axle. The flexibility of the resilient wheel can be related to ③. The formation of polygonal wheels in the considered frequency range may be likely — the three distinctive positive peaks associated with the structural modes of the wheelset may lead to corresponding predominant polygonal orders at a given speed. If there are significantly lower or even negative evolutionary tendencies directly before or after the positive peaks, e.g. ②, a more distinct formation of predominated

orders is to be expected. Note, the location (frequency) of the distinctive positive peaks in the ETCs differs between the inner and outer wheels.

Configuration B, brown line, where the axle is considered rigid and the resilient wheel flexible, exhibits only ③. At the outer wheel, the evolution tendencies increase gradually until the positive peak at 108 Hz is reached. From there, the evolution tendencies decrease drastically and turn direction at 115 Hz. The negative peak is observed at 122 Hz. Finally, the tendencies increase slowly but remain in the negative values for the frequency range of interest. At the inner wheel, the evolution tendencies increase until the positive peak at 70.5 Hz. Then, evolution tendencies turn direction at 85 Hz and the negative peak is observed at 107.2 Hz. Finally, the evolution tendencies turn positive at 130 Hz and from this point, corresponding initial OOR orders will grow in the frequency range of interest. Interestingly, the qualitative features of ③ are similar in Configuration B and Configuration D – only its location (frequency) and amplitudes change. Again, the formation of predominant orders may be expected, but now only one distinctive positive peak is present at the inner root and outer tread, respectively.

At Configuration C, purple line, where the axle is modelled flexible and the (resilient) wheel rigid, the amplitudes of ① and ② are significantly smaller than those of Configuration D, but their qualitative features are similar. ③ is not visible. At the outer wheel, the evolution tendencies are negative for low frequencies until the turning point at 6 Hz. From there, they grow gradually until the first positive peak at 19.6 Hz. Now, the tendencies decrease drastically to values close to zero before increasing to the second peak at 46.7 Hz. Again, the tendencies decrease drastically to values close to zero before they increase gradually for the remaining frequencies in the range of interest. At the inner wheel, a gradual increase of the evolution tendencies is identified at low frequencies until the first positive peak is at 20 Hz. Then, they decrease drastically to low negative values before the increase again to the second peak at 46.9 Hz. Next, the evolution tendencies turn direction at 48.4 Hz and the negative peak is observed at 49 Hz. Before the tendencies start to decrease slightly at 135 Hz, they increase gradually, turning their direction at 51.5 Hz. Here, the formation of predominant orders associated with the first and second bending modes of the wheelset may be expected. Corresponding predominant orders might not be as distinctive due to increasing evolution tendencies after ②.

It can be concluded from the discussion above that the compliance of the wheelset dominates the shape of the ETCs in the considered frequency range. A significant impact due to the compliance of the primary and secondary suspension has not been observed. Similar observations can be made at the rear wheelset. Interestingly, a combination and interaction of the wheelset axle and the resilient wheel appear to amplify the amplitudes of ① and ② significantly in contrast to the configurations, where either only the (resilient) wheel or the axle is modelled to be flexible. As a consequence, wheel polygonization might be accelerated in these frequency ranges. Modifying this interaction, e.g. by changing the effective stiffness of the wheelset axle, may influence the ETCs essentially.

Another interesting aspect is the location of the point of contact at the wheel profile in the lateral direction since different evolution tendency curves may lead to different manifestations of predominant polygonal orders on respective areas at the wheel profile. In curves with a small radius of curvature, the outer front wheel is in flange root contact, and the inner front wheel has a point of contact at the wheel tread. Their contact patches do not overlap. Consequently, their wear development may be different, see also Fig. 5. Thus, different predominant orders may be featured in the flange root than in the wheel tread and influences, as described later, may have different effects on the respective area at the wheel profile.

Note, the most influential contact responses on the phase relationship between the initial wheel OOR and wear in curves with a small radius of curvature are the lateral creepage and the normal force. The remaining contact responses have only marginal a impact. Besides the steady-state value, the ratio between the steady-state value and amplitude appear to be essential factors in how significant the individual contact response is.

Fig. 6 presents the impact of the effective stiffness c_{eff} of the wheelset axle on the ETCs. The effective stiffness c_{eff} takes the bending and the lateral elasticity of the wheelset axle into account. In addition to the baseline configuration, blue line, the stiffness has been decreased ($0.5 c_{eff}$), green line, and increased ($1.5 c_{eff}$, brown line; $2 c_{eff}$, purple line) reasonably. Increasing the effective stiffness of the wheelset axle increases the frequency of its structural modes. Accordingly, ① and ② shift their position (frequency) in the ETCs. Interestingly, the amplitudes of ① and ② increase with increasing axle stiffness. This is especially visible at the second positive peak, ②, (50 – 75 Hz), which is associated with the second bending mode of the wheelset, at the outer wheel, where the wheel is in flange root contact. At the inner wheel, where the contact position is located at the wheel treat, the first positive peak, ①, displays bigger growth of amplitude than the second peak, ②, in the ETC. A potential acceleration of the evolution of corresponding predominant orders may be expected. In contrast, the position (frequency) of ③, which is associated with the resilient wheel, remains almost identical. Its amplitudes decrease gradually as the effective stiffness of the wheelset increases. Only the impact of the effective stiffness of the wheelset axle on the ETCs is studied here, a potentially significant influence on the dynamic performance of the vehicle and ride comfort is not addressed.

So far, the impact of structural modes of the wheelset on the ETCs has been highlighted. However, several other factors may influence the evolution of the circumferential wheel wear. Contact conditions are an interesting aspect as they constantly change due to the operational conditions, vehicle dynamics, and various contact contaminations. They are studied in the next section.

3.2. Influence of contact conditions on the wear evolution

Contact responses (e.g. creepages, creep forces, and contact patch size) may vary substantially when the contact conditions change. These variations may cause subsequent wear amplitude and phase changes, which are analysed in this section.

Based on the orientation of the wheelset/bogie, the location of contact between wheel and rail may change — tread contact, flange contact, one/two-point contact, or conformal contact may emerge. The orientation of the wheelset/bogie in curves depends on several factors. In sharp curves, typical for tramway networks, the radius of curvature has a significant impact.
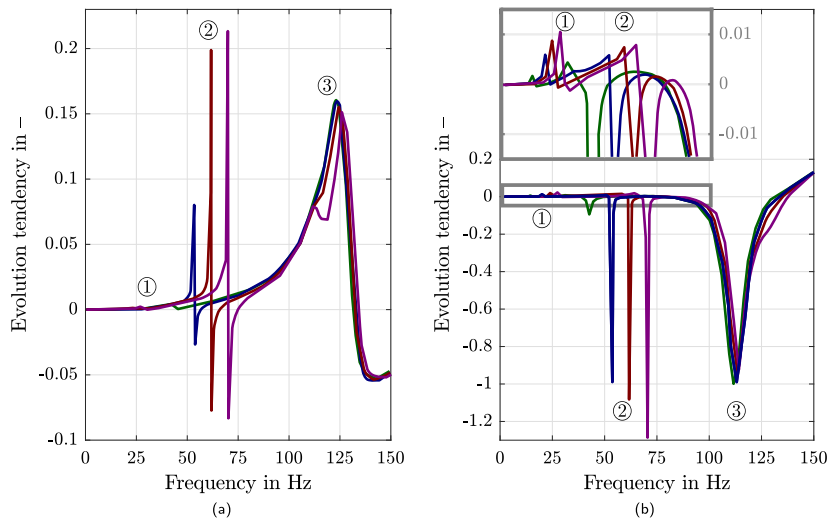
Fig. 6. Impact of effective axle stiffness on the ETCs. (a) Outer front wheel (b) Inner front wheel. $0.5\,c_{\text{eff}}$ (——), Baseline (——), $1.5\,c_{\text{eff}}$ (——), $2\,c_{\text{eff}}$ (——).
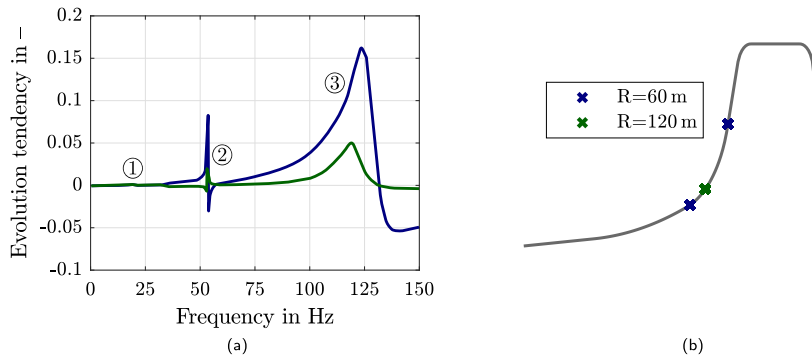

Fig. 7. Influence of contact conditions on the ETCs based on the orientation of the wheelset. (a) ETCs for the outer front wheel (b) Points of contact at the outer front wheel.

Table 3
FASTSIM/Polach parameters for wheel/rail contact.

Model parameter	Variant I	Variant II	Variant III	Variant IV
μ coefficient of friction in –	0.3	0.25	0.25	0.13
A ratio of friction coefficients μ_∞/μ_0 in –	0.4	0.4	0.4	0.4
B coefficient of exponential friction decrease in s/m	0.4	0.2	0.2	0.2
k_A in –	1	1	0.3	0.15
k_S/k_A Kalker weight ratio in –	–	–	0.5	0.334

The impact of changing points of contact on the ETC, caused by different radii of curvature, is presented for the outer wheel in Fig. 7(a). Besides the baseline ETC for a radius of curvature of R=60 m, blue, an ETC for the radius of R=120 m, green, is depicted. Fig. 7(b) shows the points of contact at the outer wheel of the leading wheelset for the two radii: two-point contact occurs at R=60 m, one-point contact at R=120 m. The location (frequency) of ① – ③ in the ETC does not change. However, the evolution tendencies show opposite directions at ② due to a significant shift of the wear phase response. Additionally, it is noted that increasing the radius of curvature results in decreasing amplitudes of ① – ③ as a consequence of decreasing wear amplitudes. An increase of corresponding predominant orders due to the positive peak at ② may still be expected.

In comparison, not illustrated here, at the inner wheel of the leading wheelset, the contact patch position remains nearly identical for both radius R=60 m and R=120 m. The evolution directions do not change, but similar to the outer wheel, the amplitudes of ① – ③ decrease with increasing radius of curvature.

To study the qualitative influence of the lateral creep force–creepage characteristics, four variants (I–IV) are considered, which are depicted in Fig. 8. To consider the remarkably reduced initial slope at the Variants III and IV, instead of [27,28] used for variant I and II, the tangential forces are calculated according to the model of Polach, [35], see also parameters given in Table 3.
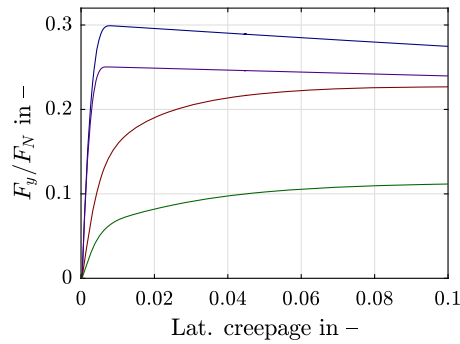
Fig. 8. Lateral creep force–creepage characteristics. (———) Variant I, (———) Variant II, (———) Variant III, (———) Variant IV.
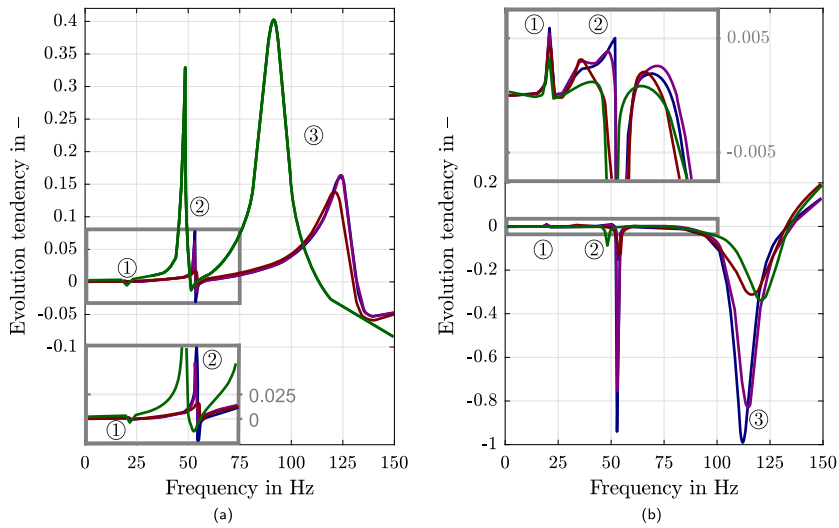

Fig. 9. Influence of the lateral creep force–creepage characteristics on the ETCs with zoomup (grey box). (a) Outer front wheel (b) Inner wheel. Variant I (———), Variant II (———), Variant III (———), Variant IV (———).

The relationship between the creepage and the contact forces, i.e. the creep force–creepage characteristics, is nonlinear and may vary significantly due to a change of the contact conditions. Basically, any contamination of the rail and/or wheel contact surfaces, e.g. fallen tree leaves, oil or rain/snow, or purposely applied adhesion enhancers, such as sand and traction gels, lubricant/frictions modifiers, will modify the characteristics [36]. The blue line, the baseline creep force–creepage characteristics, Variant I in Table 3, may be interpreted as try wheel and rail conditions. At the purple line, both the adhesion level and the magnitude of the gradient in the falling regime are reduced compared to the baseline setup. This may correspond to wet conditions (Variant II). To map a well conditioned characteristics, the brown line is introduced. Such characteristics might be achieved by the application of friction modifiers (Variant III). A regime with a negative gradient does not emerge for the lateral creepages of interest, and the adhesion level remains relatively high. Moreover, a characteristics that might be the result of naturally contaminated contact surfaces (Variant IV) due to fallen tree leaves or oil is introduced, green line. Here, the adhesion level has been reduced considerably, and a regime with a negative gradient does not emerge again for the lateral creepages of interest.

Fig. 9 points out the impact of the lateral creep force–creepage characteristics on the ETCs. The colour code corresponds to the creep force–creepage characteristics introduced in Fig. 8. The blue line depicts the ETCs for the baseline creep force–creepage characteristics, Variant I, as discussed in Section 3.1. At the purple line, Variant II, degreasing amplitudes of ① and ② are featured. At ③, the positive peaks increase slightly; the negative peaks decrease. Amplitudes of the evolution tendencies decrease essentially compared to the blue line, Variant I, at the brown line, Variant III. This is especially visible at the second positive peak, ②, at the outer front wheel, which is associated with the second bending mode of the wheelset. Note, lower absolute values of the evolution tendencies mean slower evolution speed. The contact point conditions change from two-point contact to one-point contact at the outer wheel at the green line, which is associated with a very low adhesion level, leading to considerably increased amplitudes of ① – ③ in the ETC at the outer wheel. Particularly, the positive peaks, ② and ③, which are decisive for the growth of corresponding predominant orders, grow drastically. Additionally, the location (frequency) of ① – ③ shifts to lower values. At the inner wheel, the contact point remains nearly identical, and the amplitudes of ① and ② decrease further. At ③, the positive peak decreases and the negative peak increases compared to the brown line.
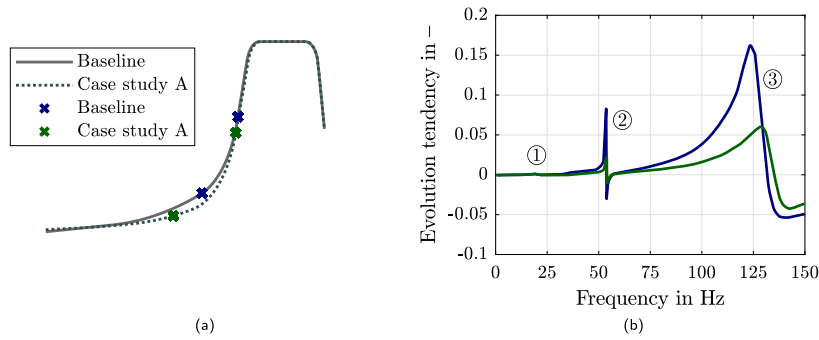
Fig. 10. Influence of wheel profile shape on ETC (a) Points of contact at the outer front wheel (b) ETCs corresponding to outer front wheel.

It can be concluded from the discussion above that lower adhesion levels may decrease the amplitudes of ① – ③ in the ETCs until an unfavourable change of the points of contact at the wheel may lead to significant increase.

To characterise the impact of the wheel/rail profile combination on the ETCs, a second wheel profile, case study A, is introduced. The rail profile remains identical. In Fig. 10(a), the points of contact at the outer wheel of the leading wheelset are depicted. As pointed out above, the outer front wheel is in flange root contact, and the inner front wheel has a point of contact at the wheel tread. The contact positions shift at the profile of case study A, green, at the outer wheel, compared to the baseline profile, blue, towards the wheel tread. This leads to significantly lower steady-state values at the normal force and lower amplitudes at the lateral creepage in case study A. As a consequence, an essential reduction in the wear amplitudes and at the amplitudes of ① – ③ in the ETC is featured at the outer wheel. The amplitudes of positive peaks, ① – ③, which are decisive for the growth of corresponding predominant orders, of case study A, green line, decrease significantly compared to the baseline setup, blue line, in the ETC at the outer wheel (wheel flange) depicted in Fig. 10(b). In contrast, the contact position at the inner wheel (wheel tread) and the ETC remains almost identical.

3.3. Influence of IRW

As mentioned before, due to the release of the rotational constraint between IRW, excitations from the initial OOR of other wheels may be viewed as random. A potential acceleration of wheel polygonization due to a specific phase shift between the OOR profiles of the right and the left wheel of a solid axle wheelset, as discussed in [34], is not to be expected. However, the wheelset loses the ability of natural curving and centring. As a result, large angles of attack may arise at straight tracks leading to an ETCs with a similar shape as in curves.

Solid axle wheelsets may experience high longitudinal creepage in curves due to the rotational constraint between the wheels. A distinct peak associated with the first torsional mode of the wheelset may arise in the ETCs as a consequence.

4. Conclusions

This paper investigates the influence of vehicle properties, characteristic for trams, on the wheel polygonal wear evolution resulting from initially out-of-round railway wheels. In particular, ETCs, predicting wheel OOR orders that would grow predominantly at a given speed, are studied. Emphasis is put on curves with a small radius of curvature, which are typical for tramway networks. Based on the results, some conclusions can be drawn.

Findings reveal that both the compliance of the wheelset axle and the resilient wheel dominates the development of potentially predominant OOR orders in the frequency range of interest. In particular, the combination and interaction of the resilient wheel and the wheelset axle appear to amplify the evolution of dominant orders associated with the first and second bending modes of the wheelset axle significantly. Interestingly, an acceleration of wheel polygonization at respective frequencies is expected when the stiffness of the axle of the wheelset increases.

Although omitted here for brevity, in straight tracks, the ETCs are dominated similarly by the structural modes of the wheelset. Narrow curves in the network may accelerate wheel polygonization significantly, as the evolution tendencies rise with decreasing radius of curvature as a consequence of increasing lateral creepage. Results reveal that purposely applied friction modifiers might be a potential method to decelerate wheel polygonization. However, at a very low level of adhesion, significantly increased growth rates of corresponding initial OOR orders may emerge in the flange root due an unfavourable change in the points of contact at the wheel. Optimizing wheel/rail profile combinations may be a feasible mitigation of wheel polygonization. At solid axle wheelsets, a distinctive peak associated with the first torsional mode of the wheelset may arise in the ETCs due to the high longitudinal creepage in curves.

The frequency of the dominant structural modes and the vehicle speed governs the wavelength of potentially predominant wheel OOR orders.

Declaration of competing interest

The authors declare that they have no known competing financial interests or personal relationships that could have appeared to influence the work reported in this paper.

Acknowledgements

References

[1] J.C. Nielsen, A. Johansson, Out-of-round railway wheels-a literature survey, Proc. Inst. Mech. Eng. F J. Rail Rapid Trans. 214 (2) (2000) 79–91.
[2] G. Tao, Z. Wen, X. Jin, X. Yang, Polygonisation of railway wheels: A critical review, Railw. Eng. Sci. (2020) 1–29.
[3] W. Zhai, X. Jin, Z. Wen, X. Zhao, Wear problems of high-speed wheel/rail systems: observations, causes, and countermeasures in China, Appl. Mech. Rev. 72 (6) (2020).
[4] S. Iwnicki, J.C. Nielsen, G. Tao, Out-of-round railway wheels and polygonisation, Veh. Syst. Dyn. (2023) 1–44.
[5] W. Shen, C. Song, G. Li, X. Li, C. Li, Research for high-speed EMU wheel hardness and polygon-form relationships with solutions, Railw. Locomot. Car 38 (4) (2018) 18–23.
[6] P. Meinke, S. Meinke, Polygonalization of wheel treads caused by static and dynamic imbalances, J. Sound Vib. 227 (5) (1999) 979–986.
[7] X. Kang, G. Chen, Q. Song, B. Dong, Y. Zhang, H. Dai, Effect of wheelset eccentricity on the out-of-round wheel of high-speed trains, Eng. Fail. Anal. 131 (2022) 105816.
[8] Y. Ye, D. Shi, P. Krause, Q. Tian, M. Hecht, Wheel flat can cause or exacerbate wheel polygonization, Veh. Syst. Dyn. 58 (10) (2020) 1575–1604.
[9] R. Fröhling, U. Spangenberg, E. Reitmann, Root cause analysis of locomotive wheel tread polygonisation, Wear 432 (2019) 102911.
[10] X. Yang, G. Tao, W. Li, Z. Wen, On the formation mechanism of high-order polygonal wear of metro train wheels: Experiment and simulation, Eng. Fail. Anal. 127 (2021) 105512.
[11] X. Wu, S. Rakheja, W. Cai, M. Chi, A. Ahmed, S. Qu, A study of formation of high order wheel polygonalization, Wear 424 (2019) 1–14.
[12] W. Cai, M. Chi, X. Wu, F. Li, Z. Wen, S. Liang, X. Jin, Experimental and numerical analysis of the polygonal wear of high-speed trains, Wear 440 (2019) 203079.
[13] C. Ma, L. Gao, R. Cui, T. Xin, The initiation mechanism and distribution rule of wheel high-order polygonal wear on high-speed railway, Eng. Fail. Anal. 119 (2021) 104937.
[14] X. Zhao, G. Chen, J. Lv, S. Zhang, B. Wu, Q. Zhu, Study on the mechanism for the wheel polygonal wear of high-speed trains in terms of the frictional self-excited vibration theory, Wear 426 (2019) 1820–1827.
[15] B. Wu, Q. Qiao, G. Chen, J. Lv, Q. Zhu, X. Zhao, H. Ouyang, Effect of the unstable vibration of the disc brake system of high-speed trains on wheel polygonalization, Proc. Inst. Mech. Eng. F J. Rail Rapid Trans. 234 (1) (2020) 80–95.
[16] F. Zehetbauer, J. Edelmann, M. Plöchl, A minimal model to study self-excited vibrations of a tram wheelset in curves with small radius of curvature, Veh. Syst. Dyn. (2023) 1–21.
[17] W. Cai, M. Chi, G. Tao, X. Wu, Z. Wen, Experimental and numerical investigation into formation of metro wheel polygonalization, Shock Vib. 2019 (2019).
[18] A. Johansson, C. Andersson, Out-of-round railway wheels—a study of wheel polygonalization through simulation of three-dimensional wheel–rail interaction and wear, Veh. Syst. Dyn. 43 (8) (2005) 539–559.
[19] J. Mu, J. Zeng, C. Huang, Y. Sun, H. Sang, Experimental and numerical investigation into development mechanism of wheel polygonalization, Eng. Fail. Anal. 136 (2022) 106152.
[20] B. Suarez, J. Chover, P. Rodriguez, F.J. González, Effectiveness of resilient wheels in reducing noise and vibrations, Proc. Inst. Mech. Eng. F J. Rail Rapid Trans. 225 (6) (2011) 545–565.
[21] B. Morys, Enlargement of out-of-round wheel profiles on high speed trains, J. Sound Vib. 227 (5) (1999) 965–978.
[22] B. Peng, S. Iwnicki, P. Shackleton, Y. Song, General conditions for railway wheel polygonal wear to evolve, Veh. Syst. Dyn. (2019) 1–20.
[23] B. Fu, S. Bruni, S. Luo, et al., Numerical simulation for polygonal wear of railway wheels, in: 11th International Conference on Contact Mechanics and Wear of Rail/Wheel Systems, CM 2018, 2018, pp. 271–280.
[24] F. Zehetbauer, J. Edelmann, M. Plöchl, F. Magerl, Study on potential evolution mechanisms of OOR wheels at trams, in: Advances in Dynamics of Vehicles on Roads and Tracks II. IAVSD, in: Lecture Notes in Mechanical Engineering, Springer, 2021, pp. 572–581.
[25] Simpack, release 2019, 2022, https://www.3ds.com/de/produkte-und-services/simulia/produkte/simpack/. (Accessed 12 05 2022).
[26] H. Hertz, Über die Berührung fester elastischer Körper, Walter de Gruyter, Berlin/New York Berlin, New York, 1882.
[27] J. Kalker, A fast algorithm for the simplified theory of rolling contact, Veh. Syst. Dyn. 11 (1) (1982) 1–13.
[28] O. Polach, Influence of locomotive tractive effort on the forces between wheel and rail, Veh. Syst. Dyn. 35 (1) (2001) 7–22.
[29] B. Peng, S. Iwnicki, P. Shackleton, D. Crosbee, Comparison of wear models for simulation of railway wheel polygonization, Wear 436 (2019) 203010.
[30] T. Jendel, M. Berg, Prediction of wheel profile wear: Methodology and verification, Veh. Syst. Dyn. 37 (sup1) (2002) 502–513.
[31] R. Enblom, M. Berg, Simulation of railway wheel profile development due to wear—influence of disc braking and contact environment, Wear 258 (7–8) (2005) 1055–1063.
[32] J. Archard, Contact and rubbing of flat surfaces, J. Appl. Phys. 24 (8) (1953) 981–988.
[33] W. Cai, X. Wu, M. Chi, C. Yang, H. Huang, Wheel polygonisation growth due to multiple wheelsets/track coupling vibration, Veh. Syst. Dyn. (2022) 1–23.
[34] M. Meywerk, Polygonalization of railway wheels, Arch. Appl. Mech. 69 (2) (1999) 105–120.
[35] O. Polach, Creep forces in simulations of traction vehicles running on adhesion limit, Wear 258 (7–8) (2005) 992–1000.
[36] E. Vollebregt, K. Six, O. Polach, Challenges and progress in the understanding and modelling of the wheel–rail creep forces, Veh. Syst. Dyn. 59 (7) (2021) 1026–1068.